Estimating LST Using a Vegetation-Cover-Based Thermal Sharpening Technique

Yitong Jiang and Qihao Weng, *Member, IEEE*

***Abstract*—Vegetation-cover-based thermal sharpening techniques have mostly been developed and tested in agricultural areas. Overlooking the impact of soil moisture on surface temperatures is a common problem in these algorithms. This letter developed a vegetation thermal sharpening method for the City of Indianapolis, Indiana, USA, and estimated land surface temperature by disaggregated Landsat Thematic Mapper thermal infrared data from 120 to 30 m. The root-mean-square error was yielded at 1.90 °C and 1.91 °C using NDVI and fractional vegetation cover as predictors, respectively. The error of the estimation was overlaid with a soil moisture map, which was derived based on the surface energy balance modeling. The pixels with large errors were largely distributed in the areas with low soil moisture. These areas were covered by impervious surfaces such as major roads, commercial land, and the airport. This result suggested that in the urban areas, besides vegetation cover and soil moisture, impervious surfaces must be incorporated in developing any future thermal sharpening techniques. The incorporation of population density and per capita consumption of energy may provide further improvements in the estimation.**

***Index Terms*—Impervious surfaces, land surface temperature (LST), Landsat, soil moisture, thermal sharpening, urban areas, vegetation fraction.**

I. Introduction

THE NEED of high-spatial-resolution thermal infrared (IR) images and the obstacles for obtaining such data directly from satellite sensors have been clearly addressed by [1]–[4]. Two major approaches of thermal sharpening have been developed. An emissivity-based method has been applied in the urban areas [5], and a vegetation-cover-based method has been applied in the agricultural areas [2], [3], [6], [7]. In this letter, the vegetation-cover-based method was tested in an urban area in the Midwest region of the USA. This method was based on the assumption that vegetation cover is the primary driver of land surface temperature (LST) variation. This may be true in an area with fair amount of vegetation cover. Research on the temperature–vegetation index (TVX) space found that the variation of LST correlated with moisture availability at a fixed amount of vegetation cover [8]. Therefore, to better interpret the estimated temperatures from the vegetation-cover-based thermal sharpening method, soil moisture needs to be considered. The objectives of this letter are: 1) to estimate LST by disaggregating the thermal IR image from Landsat Thematic Mapper (TM) sensor from 120 to 30 m in the urban and suburban areas in Indianapolis using the vegetation-cover-based method; and 2) to interpret the estimated result with reference to soil moisture data. The implication of the thermal sharpening technique for future urban studies was further discussed.

Manuscript received January 25, 2013; revised February 27, 2013; accepted March 13, 2013. Date of publication April 30, 2013; date of current version June 13, 2013.

The authors are with the Center for Urban and Environmental Change, Department of Earth and Environmental Systems, Indiana State University, Terre Haute, IN 47809 USA (e-mail: qweng@indstate.edu).

Color version of one or more figures in this paper are available online at http://ieeexplore.ieee.org.

Digital Object Identifier 10.1109/LGRS.2013.2257667

II. Data and Methodology

A. Study Area and Data

The chosen study area was Marion County (i.e., the city proper of Indianapolis), Indiana, USA. A population of 860 454 in year 2000 made it the largest county in Indiana. It is located at the center of the State of Indiana on a flat plain. According to the National Land Cover Database 2001, the major land-cover types included developed areas, cultivated crops, forest, and open water. The variation of land-cover types made Marion County suitable for urban remote sensing studies, particularly in interpreting the LST spatial variation and analyzing major factors. A Landsat TM image (Path 21 Row 32) was acquired on July 6, 2002, under clear weather condition for the study.

B. Data Preparation

Atmospheric effect on bands 1–5 and 7 was corrected by a simplified dark object subtraction method, which assumed no atmospheric transmittance loss and no diffuse downward radiation at the surface [9]. LST was retrieved by the following steps. First, a digital number on the TM thermal IR band was converted to at-sensor radiance according to the referenced values from Chander *et al.* [10]; second, band average atmospheric transmission, effective bandpass upwelling radiance, and downwelling radiance were calculated using the Atmospheric Correction Parameter Calculator [11]; third, land surface emissivity was estimated with the normalized difference vegetation index (NDVI) method [12]; and finally, LST was retrieved by employing the radiative transfer equation [13].

NDVI and fractional vegetation cover were computed as two indicators of vegetation cover. Linear spectral mixture analysis was used for the fractional vegetation cover computation. Details about the selection of endmembers and the estimation of the fraction have been discussed by Weng *et al.* [14].

C. Thermal Sharpening

The three-step vegetation-cover-based LST estimation method was adopted from Kustas *et al.* [2] and Agam *et al.* [3]. First, the linear regressions between observed LST and vegetation cover were performed at 120 m, and the LST at 120 m was estimated by the regressions

$$f_{120} = f(VC_{120}) \tag{1}$$

where $\hat{T}_{120}$ is the estimated LST at 120 m, and VC_{120} is vegetation cover at 120 m, including NDVI and vegetation fraction. The Landsat TM image that was downloaded from USGS website had been preprocessed to a spatial resolution of 30 m for all bands. Therefore, bands 3, 4, and 6 were resampled from 30 to 120 m using nearest neighbor interpolation before the first step. After the resampling, the observed LST at 120 m was retrieved by the same method discussed in data preparation section.

Second, the residual of estimated LST at 120 m was calculated by subtracting estimated LST from observed LST. The equation for calculating the residual can be expressed as

$$\Delta\hat{T}_{120} = T_{120} - \hat{T}_{120} \tag{2}$$

where $\Delta\hat{T}_{120}$ is the residual of estimated LST, T_{120} is the observed LST, and $\hat{T}_{120}$ is the estimated LST at 120 m.

Third, the regression equations at 120 m from the first step were applied at 30 m, and the residual from the second step was added back to the sharpened image

$$\hat{T}_{30} = f(VC_{30}) + \Delta\hat{T}_{30} \tag{3}$$

where $\hat{T}_{30}$ is the estimated LST at 30 m, and $f(VC_{30})$ is the estimated LST from the LST–vegetation cover regression at 30 m. The residual of the estimated LST at 120 m was resampled to 30 m and was then written as $\Delta\hat{T}_{30}$.

The above sharpening procedure was applied on both urban and suburban areas. Interstate Highway 465 was used to separate the urban area from the suburban area. The typical urban land use and land-cover types such as commercial, industrial, and high- and medium-density residential areas were mainly distributed in the circle of Interstate Highway 465, whereas suburban land-cover types such as agricultural fields, forestry, and low-density residential area were located between Interstate Highway 465 and the county boundary.

The level of accuracy between estimated and observed LSTs at 30 m was assessed by the root-mean-square error (RMSE). The observed LST was retrieved from the TM thermal IR band on the same image at 30 m

$$\text{RMSE} = \sqrt{\frac{\sum_{i=1}^{n}(\hat{T} - T)^2}{n}} \tag{4}$$

where $\hat{T}$ is the estimated temperature, and T is the observed temperature.

D. Soil Moisture Computation

Soil moisture was retrieved based on the surface energy balance modeling. As evaporation was the major source of latent heat flux, the evaporative fraction can be estimated by

$$\text{Evaporative Fraction} = \varphi \times \frac{\Delta}{\Delta + \gamma} \tag{5}$$

where φ is the extension of the Priestley–Taylor parameter α, and $\Delta/\Delta + \gamma$ is the air temperature control parameter [15]. In this letter, the maximum value of φ (under wet surface condition) was assumed to be 1.26, and the minimum is 0. $\Delta/\Delta + \gamma$ was estimated using a linear function with air temperature [16]. We assumed that the air temperature was consistent for the whole study area. φ_i represented the φ value of a random pixel. The method to interpolate φ_i in the triangular scatterplot in the TVX space was shown in Fig. 1.

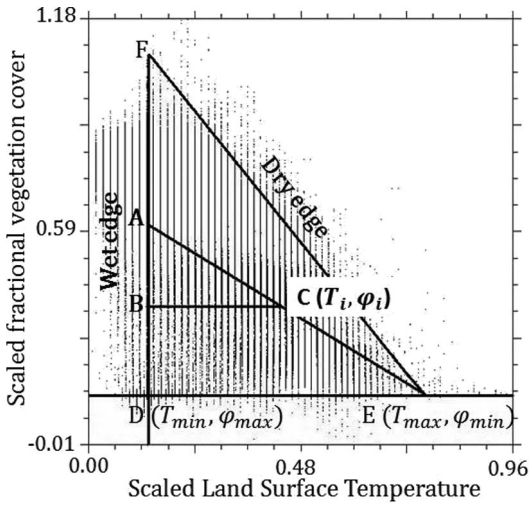

Fig. 1. Method to interpolate φ_i. φ_i is the φ value for a random pixel in the TVX space. In similar triangles ABC and ADE, we have AC/AE = BC/DE. φ_i can be calculated using the values of $T_{\min}$, $T_{\max}$, T_i, $\varphi_{\max}$, and $\varphi_{\min}$.

The detailed description of the TVX space could be found in Carlson and Arthur [8]. In this case, point E represents the pixel with the highest temperature and lowest φ value, and point D represents the pixel with the lowest temperature and highest φ value. Point A has the highest φ value because it is on the wet edge. In similar triangles ABC and ADE, we have AC/AE = BC/DE. Therefore, φ_i can be written as

$$\varphi_i = \frac{T_{\max} - T_i}{T_{\max} - T_{\min}} (\varphi_{\max} - \varphi_{\min}) + \varphi_{\min} \tag{6}$$

where $T_{\max}$ is the maximum scaled LST, and $T_{\min}$ is the minimum. $\varphi_{\max}$ is the maximum φ value, and $\varphi_{\min}$ is the minimum. T_i and φ_i are the LST and φ value of a random pixel. LST was transformed to scaled LST before the TVX space was formed. The equation for transforming LST to scaled LST was written as

$$T^* = \frac{T - T_{\min}}{T_{\max} - T_{\min}}. \tag{7}$$

The method to calculate soil moisture from evaporation fraction was adapted from Lee and Pielke [17]

$$\theta = \frac{\theta_{\text{fc}} \times \arccos(1 - \sqrt{4 \times \text{EF}})}{\pi} \tag{8}$$

where θ is volumetric soil moisture, and θ_{fc} is volumetric soil moisture at field capacity. Silt loam and clay loam were commonly found in our study area. Based on soil–water characteristics of different soil types in [17], θ_{fc} was assumed to be 0.3. The soil moisture image was then compared with the squared difference between estimated and observed LSTs.

III. Results

The RMSEs were 1.90 °C and 1.91 °C in the urban area using NDVI and vegetation fraction as predictors, respectively. The estimated LST yielded smaller RMSEs in the urban than in the suburban area (2.04 °C and 1.96 °C in the suburban area using NDVI and vegetation fraction, respectively). This result implies that the vegetation-cover-based thermal sharpening method is effective in the urban areas. The estimated LST from NDVI and vegetation fraction regression were highly similar in the urban area. Small [18] stated that a subpixel technique was more suitable in observing and extracting relatively fine urban surface features. However, in this experiment, the fractional vegetation cover did not show its advantage in estimating LST. The accuracy of vegetation fraction may need to be improved.

Relatively large RMSE (2.04 °C) in the suburban area was resulted from the NDVI regression. This may be due to the insensitivity of NDVI in monitoring the vegetation cover when the ground surface was fully covered by leaves. Based on Carlson and Ripley [19], NDVI rapidly increased with fractional vegetation cover until reaching a full covering threshold when fractional vegetation cover equaled to 1 and NDVI stayed around 0.7. In this experiment, the largest NDVI value was observed at 0.8. Dense vegetated areas as forestry and agricultural land were located in the suburban area. The deficiency of measuring vegetation cover by NDVI led to a relatively high RMSE.

The squared difference between estimated and observed LSTs was calculated by $(\hat{T}-T)^2$ for each pixel, where $\hat{T}$ is the estimated LST and T is the observed LST. In using NDVI as a predictor, when $\hat{T}-T>0$, the mean of $(\hat{T}-T)^2$ was 7.80 °C with a standard deviation of 17.38 °C; when $\hat{T}-T<0$, the mean of $(\hat{T}-T)^2$ was 4.13 °C with a standard deviation of 13.84 °C. In using vegetation fraction as a predictor, when $\hat{T}-T>0$, the mean of $(\hat{T}-T)^2$ was 3.44 °C with a standard deviation of 10.76 °C; when $\hat{T}-T<0$, the mean of $(\hat{T}-T)^2$ was 4.10 °C with a standard deviation of 13.58 °C. The soil moisture ranged from 2% to 24%, with a mean of 19% and a standard deviation of 1%. The areas with higher soil moisture were forest, agricultural, and riparian corridors, and the areas with lower soil moisture were located in the well-developed urban areas.

In Fig. 2, the green and yellow pixels were the ones with a $(\hat{T}-T)^2$ larger than the sum of the mean and one standard deviation, but green ones had positive $(\hat{T}-T)$, whereas yellow ones possessed negative $(\hat{T}-T)$. The spatial distribution of relatively large $(\hat{T}-T)^2$ estimated from NDVI and vegetation fraction shared a similar pattern. Therefore, in Fig. 2, we chose the results from using NDVI as the predictor as an example. In Fig. 2(a), some of the pixels with large errors were distributed along water bodies and riparian corridors, where soil moisture

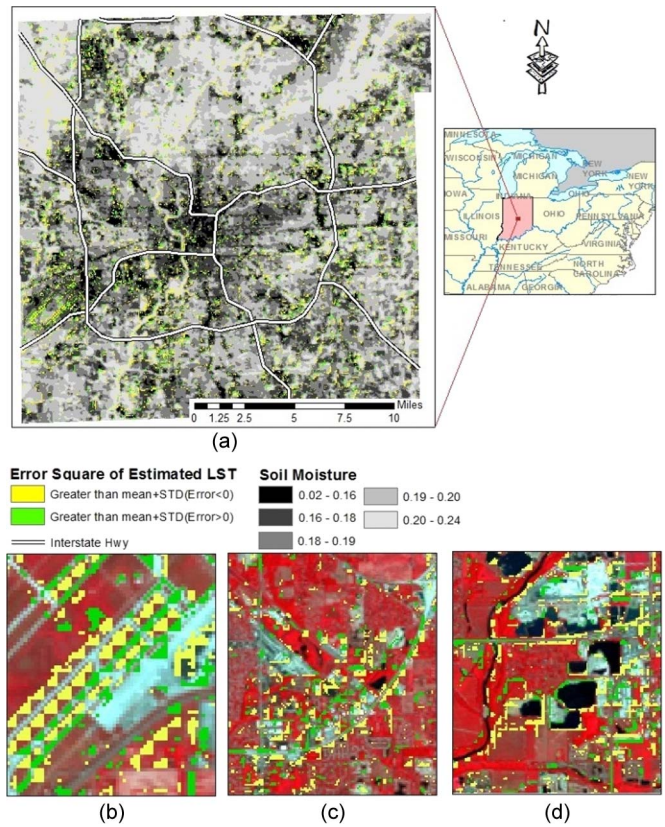

Fig. 2. Distribution of larger errors of estimated LST from NDVI over the soil moisture map. In the three selected areas (b), (c), and (d), green pixels have positive $\hat{T}-T$, whereas yellow pixels have negative $\hat{T}-T$. (a) Estimated LST errors over the soil moisture map. (b) Airport. (c) Developed area and highway curves. (d) Along highway and water bodies.

was high. However, the majority of the pixels with large errors were located in the developed lands with low soil moisture. This result shows the strong impact of impervious surfaces on LST and the drawback of using only vegetation cover as the parameter to estimate LST in the urban areas.

In Fig. 2(b) and (c), the yellow pixels were located along the runways of the airport and the curves of major highways. The size of yellow pixels was mainly 4×4 pixels, which equaled to the size of the unsharpened 120-m pixels. The mixed pixels at the coarse resolution (120 m in this case) were mainly distributed along the runways and major highways. This finding indicates that the direction and geometry of specific land features may impact the accuracy of LST estimation, and mixed pixels in the coarse resolution image due to the geometry of these land features is an obstacle in LST estimation. We also noticed in Fig. 2(c) and (d) that more green pixels $(\hat{T}-T>0)$ were located right on the impervious surfaces, whereas yellow ones $(\hat{T}-T<0)$ were near impervious surfaces scattering on vegetated or bare ground. This finding indicates that LST estimation using linear regression between LST and vegetation cover may overestimate LST for the built-up areas and underestimate LST in dense vegetated and high-moisture areas.

IV. Conclusion and Discussions

This letter has employed a vegetation-cover-based thermal sharpening technique to estimate LST at 30 m using Landsat

TM thermal IR data. We applied it to an urban area and a suburban area in the City of Indianapolis, USA. The RMSEs of 1.90 °C and 1.91 °C in the urban area and 2.04 °C and 1.96 °C in the suburban area were achieved, respectively, when NDVI and vegetation fraction regression were applied. Overall, the method was found effective. When the distribution of large-error pixels of estimated temperature was superimposed over the soil moisture map, the characteristics of urban land cover, particularly the artificial materials, mixture of natural and man-made land cover, and the geometry of land features, and their impacts on LST were demonstrated. The main contributions of this letter include the application of a paradigm in agriculture remote sensing to the urban and suburban areas and the examination of common problems associated with the vegetation-cover-based thermal sharpening method.

The urbanization process blurred the urban and rural boundary. Therefore, methods suitable for agricultural or forestry areas are worth testing and may be optimized for urban areas, particularly for the rural–urban fringes. Our results showed that it was hard to achieve an accurate estimation of LST from disaggregating mixed pixels at coarser resolution to relatively pure pixels at finer resolution due to the heterogeneity of urban landscapes, the geometry of impervious surfaces, and the operational scales of urban land features. To differentiate impervious surface from adjacent land-cover types (e.g., bare soil) is crucial in dealing with the mixed pixels. Fractions of impervious surface and bare soil may need to be incorporated into the models because they bear different contributions to LST.

Estimating soil moisture from the TVX space may bring in bias because soil moisture values were mainly determined by relating LST to vegetation cover values. In the urbanization process, various vegetated surfaces were replaced by impervious surfaces. Thus, the effectiveness of using the TVX space to derive soil moisture in urban areas needs to be re-evaluated, particularly in the high-intensity built-up areas. Evapotranspiration, precipitation, and urban runoff may be derived from satellite images, and they can be also related to the urban moisture conditions. Therefore, using these variables to classify the study area prior to running the thermal sharpening algorithm may be a suitable way to improve the sharpening method. The TVX space indicated that, when vegetation cover amount was relatively constant, other factors such as moisture condition became more significant. Therefore, the variation of vegetation cover was key to a successful application of the method. In the areas of dense forestry, moisture condition controlled the temperature variation, whereas in agriculture areas, vegetation cover was the main controlling factor due to the variation of vegetation coverage in harvested and planted fields. In contrast, in sparse vegetated developed areas, energy released from air conditioners and cars, as well as impervious materials and composition may become the main factors for temperature variations. Anthropogenic heat should be considered in the LST estimation in the urban areas [20]. For example, population density and per capita consumption of electricity or fuels may be used as additional variables to adjust estimated LSTs [21].

REFERENCES

[1] T. J. Schmugge, W. P. Kustas, and K. S. Humes, "Monitoring land surface fluxes using ASTER observations," *IEEE Trans. Geosci. Remote Sens.*, vol. 36, no. 5, pp. 1421–1430, Sep. 1998.

[2] W. P. Kustas, J. M. Norman, M. C. Anderson, and A. N. French, "Estimating subpixel surface temperatures and energy fluxes from the vegetation index–radiometric temperature relationship," *Remote Sens. Environ.*, vol. 85, no. 4, pp. 429–440, Jun. 2003.

[3] N. Agam, W. P. Kustas, M. C. Anderson, F. Li, and C. M. U. Neale, "A vegetation index based technique for spatial sharpening of thermal imagery," *Remote Sens. Environ.*, vol. 107, no. 4, pp. 545–558, Apr. 2007.

[4] Q. Weng, "Thermal infrared remote sensing for urban climate and environmental studies: Methods, applications, and trends," *ISPRS J. Photogramm. Remote Sens.*, vol. 64, no. 4, pp. 335–344, Jul. 2009.

[5] J. Nichol, "An emissivity modulation method for spatial enhancement of thermal satellite images in urban heat island analysis," *Photogramm. Eng. Remote Sens.*, vol. 75, no. 5, pp. 547–556, May 2009.

[6] O. Merlin, B. Dchemin, O. Hagolle, F. Jacob, B. Coudert, G. Chehbouni, G. Dedieu, J. Garatuza, and Y. Kerr, "Disaggregation of MODIS surface temperature over an agricultural area using a time series of Formosat-2 images," *Remote Sens. Environ.*, vol. 114, no. 11, pp. 2500–2512, Nov. 2010.

[7] C. Jeganathan, N. A. S. Hamm, S. Mukherjee, P. M. Atkinson, P. L. N. Raju, and V. K. Dadhwal, "Evaluating a thermal image sharpening model over a mixed agricultural landscape in India," *Int. J. Appl. Earth Observ. Geoinf.*, vol. 13, no. 2, pp. 178–191, Apr. 2011.

[8] T. N. Carlson and S. T. Arthur, "The impact of land use–land cover changes due to urbanization on surface microclimate and hydrology: A satellite perspective," *Global Planet. Change*, vol. 25, no. 1/2, pp. 49–65, Jul. 2000.

[9] C. Song, C. E. Woodcock, K. C. Seto, M. P. Lenney, and S. A. Macomber, "Classification and change detection using Landsat TM data: When and how to correct atmospheric effects?" *Remote Sens. Environ.*, vol. 75, no. 2, pp. 230–244, Feb. 2001.

[10] G. Chander, B. L. Markham, and D. L. Helder, "Summary of current radiometric calibration coefficients for Landsat MSS, TM, ETM +, and EO-1 ALI sensors," *Remote Sens. Environ.*, vol. 113, no. 5, pp. 893–903, May 2009.

[11] J. A. Barsi, J. F. Schott, F. D. Palluconi, and S. J. Hook, "Validation of a web-based atmospheric correction tool for single thermal band instruments," in *Proc. SPIE Earth Observ. Syst. X*, Aug. 2005, vol. 5882, p. 58820E.

[12] J. A. Sobrino, J. C. Jimenez-Munoz, and L. Paolini, "Land surface temperature retrieval from LANDSAT TM 5," *Remote Sens. Environ.*, vol. 90, no. 4, pp. 434–440, Apr. 2004.

[13] T. Schmugge, S. J. Hook, and C. Coll, "Recovering surface temperature and emissivity from thermal infrared multispectral data," *Remote Sens. Environ.*, vol. 65, no. 2, pp. 121–131, Aug. 1998.

[14] Q. Weng, X. Hu, and D. Lu, "Extracting impervious surfaces from medium spatial resolution multispectral and hyperspectral imagery: A comparison," *Int. J. Remote Sens.*, vol. 29, no. 11, pp. 3209–3232, Jun. 2008.

[15] L. Jiang and S. Islam, "Estimation of surface evaporation map over southern Great Plains using remote sensing data," *Water Resourc. Res.*, vol. 37, no. 2, pp. 329–340, Feb. 2001.

[16] K. C. Wang, Z. Q. Li, and M. Cribb, "Estimation of evaporative fraction from a combination of day and night land surface temperatures and NDVI: A new method to determine the Priestley–Taylor parameter," *Remote Sens. Environ.*, vol. 102, no. 3/4, pp. 293–305, Jun. 2006.

[17] T. J. Lee and R. A. Pielke, "Estimating the soil surface specific humidity," *J. Appl. Meteorol.*, vol. 31, no. 5, pp. 480–484, May 1992.

[18] C. Small, "Estimation of urban vegetation abundance by spectral mixture analysis," *Int. J. Remote Sens.*, vol. 22, no. 7, pp. 1305–1334, May 2001.

[19] T. N. Carlson and D. A. Ripley, "On the relation between NDVI, fractional vegetation cover, and leaf area index," *Remote Sens. Environ.*, vol. 62, no. 3, pp. 241–252, Dec. 1997.

[20] D. J. Sailor and L. Lu, "A top-down methodology for developing diurnal and seasonal anthropogenic heating profiles for urban areas," *Atmosp. Environ.*, vol. 38, no. 17, pp. 2737–2748, Jun. 2004.

[21] Q. Weng, D. Lu, and B. Liang, "Urban surface biophysical descriptors and land surface temperature variations," *Photogramm. Eng. Remote Sens.*, vol. 72, no. 11, pp. 1275–1286, Nov. 2006.